

Ferromagnetism and electronic structure of TmB_2

T. Mori,^{1,2,*} T. Takimoto,² A. Leithe-Jasper,² R. Cardoso-Gil,² W. Schnelle,² G. Auffermann,² H. Rosner,² and Yu. Grin²

¹International Center for Materials Nanoarchitectonics (MANA), National Institute for Materials Science (NIMS), Namiki 1-1, Tsukuba, 305-0044, Japan

²Max-Planck-Institut für Chemische Physik fester Stoffe, Nöthnitzer Str. 40, 01187 Dresden, Germany

(Received 2 April 2008; revised manuscript received 13 February 2009; published 19 March 2009)

The magnetic properties and electronic structure of thulium diboride were investigated as it is a magnetically unknown phase between ferromagnetic (FM) REB_2 ($\text{RE}=\text{Tb, Dy, Ho, Er}$) and antiferromagnetic YbB_2 . TmB_2 adopts the AlB_2 -type crystal structure ($P6/mmm$) with $a=3.26016(5)$ Å and $c=3.75351(8)$ Å and exhibits long-range FM order with the specific heat C_p exhibiting a peak at $T_C=7.2$ K at the Curie temperature. A Curie-Weiss fit of the magnetic susceptibility yielded $\mu_{\text{eff}}=7.49\mu_B/\text{Tm}$ (Tm^{3+}) and weak FM interactions. A Schottky anomaly in C_p was used to investigate crystal electric field (CEF) effects. From a measurement of $C_p(T)$ of the isostructural LuB_2 the magnetic entropy S_{mag} of TmB_2 is determined. The ordered state of the Tm ions involves three CEF levels. Electronic-structure calculations, performed within the local spin density approximation, indicate a Ruderman-Kittel-Kasuya-Yoshida-type mechanism for the magnetic order. With respect to the total energy, ferromagnetic order is found to be more stable than the A-type antiferromagnetically ordered state, in agreement with the experiment.

DOI: 10.1103/PhysRevB.79.104418

PACS number(s): 75.50.Cc, 71.20.Lp

I. INTRODUCTION

The rare-earth borides such as tetraborides REB_4 (RE = rare-earth metal), hexaborides REB_6 , and dodecaborides REB_{12} have attracted a lot of attention over the years as a rich class of materials which exhibit various phenomena of f -electron magnetism.^{1–5} Recently, new interesting aspects of the magnetism of these well-known borides have been discovered.^{6–8} Incidentally, the magnetic behavior has been investigated in higher borides which contain the B_{12} icosahedra as a structural building block.¹ Magnetism in these higher borides varies from dimerlike magnetic transitions along a one-dimensional RE chain in REB_{50} and $\text{REB}_{44}\text{Si}_2$,^{9–11} two-dimensional spin-glass behavior in REB_{17}CN , $\text{REB}_{22}\text{C}_2\text{N}$, and $\text{REB}_{28.5}\text{C}_4$ (Refs. 12–15) to three-dimensional long-range order in $\text{GdB}_{18}\text{Si}_5$.¹⁶ Although these are magnetically dilute f -electron insulators, surprisingly strong magnetic coupling has been observed, e.g., antiferromagnetic (AFM) ordering at $T_N=17$ K for TbB_{50} ,¹⁷ spin-glass freezing at $T_f=29$ K for HoB_{17}CN .¹²

However, the magnetism of the diborides, REB_2 , has not been as comprehensively reported. Ferromagnetic (FM) transitions were first observed for TbB_2 , DyB_2 , HoB_2 , and ErB_2 .⁵ Recently, YbB_2 was reported to undergo an antiferromagnetic transition.¹⁸ We have been investigating the thulium aluminoboride TmAlB_4 (YCrB_4 -type crystal structure $Pbam$), which shows multiple transitions below the first AFM ordering.¹⁹ The origin of this interesting behavior was revealed to be due to intrinsic building defects arising from the existence of a closely related structure, the ThMoB_4 -type ($Cmmm$).²⁰ In the course of this study we were successful in synthesizing the thulium diboride. Since TmB_2 lies between the FM REB_2 ($\text{RE}=\text{Tb, Dy, Ho, Er}$) and the AFM YbB_2 and its magnetic properties are unknown up to now, we elucidate the magnetic properties of TmB_2 in this paper.

II. SYNTHESIS, METHODS, AND CRYSTAL STRUCTURE

Three samples with the nominal compositions $\text{TmB}_{1.5}$, TmB_2 , and $\text{TmB}_{2.5}$ were prepared. Mixtures of thulium

(Ames, 99.9 wt. %) filings and boron powder (crystalline, Chempur, 99.999 wt. %) were cold compacted without the use of lubricants in steel dies. All experimental steps were carried out within an Ar gas glovebox system (oxygen, water impurities <1 ppm). The specimens were placed into tungsten crucibles which were sealed into tantalum tubes and slowly heated up to 1450 °C and kept there for 36 h. After annealing the furnace was switched off and the samples cooled to ambient temperature. Dense samples were achieved and no reaction with the crucible material could be detected. In order to determine the magnetic entropy, LuB_2 was also successfully synthesized as a nonmagnetic isostructural analog by similar methods.

Chemical analysis was carried out with inductively coupled plasma atomic emission spectroscopy (ICP-AES) where the samples were dissolved in acid prior to analyzing. Samples were characterized by using powder x-ray diffraction (XRD) measurements with $\text{Cu } K\alpha_1$ radiation ($\lambda = 1.54060$ Å) on a STOE-STADIP-MP diffractometer in reflection mode.

Magnetization (dc) was measured by using a Quantum Design superconducting quantum device (SQUID) magnetometer from 1.8 to 400 K and magnetic fields up to 70 kOe. Heat-capacity measurements were made using a Quantum Design PPMS with a transient heat-pulse method from zero field up to 90 kOe. The magnetic and CEF contribution was determined as the difference of $C_p(T)$ of TmB_2 and LuB_2 . Due to the small lattice specific heat of both compounds and bad thermal contact between the samples and the calorimeter platform the inaccuracy of the C_{mag} became large above ≈ 40 K.

To investigate the electronic structure of TmB_2 , a full-potential nonorthogonal local-orbital (FPLO) calculation scheme²¹ within the local (spin) density approximation [L(S)DA] was used. The experimental lattice parameters determined from our crystal structure analysis were applied. In the spin-polarized scalar-relativistic calculations the exchange and correlation potentials of Perdew and Wang²²

were used. As the basis set, Tm ($4f$, $5s$, $5p$, $6s$, $6p$, $5d$) and B ($2s$, $2p$, $3d$) states were employed. The lower-lying states were treated fully relativistically as core states. The treatment of the semicorelike states Tm ($4f$, $5s$, $5p$) as valence states was necessary to account for otherwise non-negligible core-core overlaps.

For a correct description of the correlated $4f$ states the explicit treatment of the strong Coulomb repulsion was modeled within the LSDA+ U approximation using the atomic limit double-counting scheme.²³ A typical value for localized $4f$ electrons of $U=8$ eV has been applied.²⁴ A change in U within the physically reasonable range ($U=6, 8, 10$ eV) showed no influence of the U value on the bands and the electronic density of states (DOS) in vicinity of the Fermi level. Spatial extension of the basis orbitals, controlled by a confining potential $(r/r_0)^4$, was optimized with respect to the total energy.²⁵ A dense k mesh of $24 \times 24 \times 12$ points in the irreducible part of the Brillouin zone was used to ensure accurate density of states and band-structure information, especially in the region close to the Fermi level.

The powder XRD pattern of the sample with the nominal stoichiometric composition TmB_2 was completely indexed with a hexagonal lattice and lattice parameters $a=3.26016(5)$ Å and $c=3.75351(8)$ Å obtained by least-squares refinement from the diffraction angles of 21 reflections with $2\theta \leq 116^\circ$. Whereas the parameter a is in good agreement with the literature data [cf. $a=3.2573(4)$ Å, $c=3.7473(6)$ Å,²⁶ $a=3.261$ Å, $c=3.755$ Å;²⁷ $a=3.258(3)$ Å, $c=3.745(3)$ Å,²⁸] the value of parameter c agrees well only with the data of Ref. 27 but differs noticeably from both other results, which may suggest a narrow homogeneity range of the compound. Therefore, the lattice parameters of the AlB_2 -type phase were refined also in the two-phase samples with the nominal compositions $\text{TmB}_{1.5}$ [$a=3.2611(2)$ Å, $c=3.7543(4)$ Å, in equilibrium with thulium] and $\text{TmB}_{2.5}$ [$a=3.2616(2)$ Å, $c=3.7553(3)$ Å, in equilibrium with TmB_4]. The lattice parameters of the AlB_2 -type phase in all three samples investigated are equal within 3 estimated standard deviation (e.s.d.), revealing the practically constant composition of the target phase (“line” compound).

The refinement of the crystal structure was done using the x-ray powder-diffraction data. Applying the Rietveld procedure leads to the final residuals $R_7=0.061$ and $R_p=0.074$ (Fig. 1, top). The final model is as follows: structure-type AlB_2 , space group $P6/mmm$; Tm in $(0,0,0)$, $B_{\text{eq}}=0.60(3)$ Å⁻²; B in $(\frac{1}{3}, \frac{2}{3}, \frac{1}{2})$, $B_{\text{iso}}=0.4(2)$ Å⁻² (Fig. 1, bottom). Refinement of the occupation parameter for the boron position at this stage yielded the value of 0.95(2) and the total composition $\text{TmB}_{1.90(4)}$. This is in surprising good agreement with the composition $\text{TmB}_{1.93(4)}$ obtained from chemical analysis of the sample with nominal composition TmB_2 . Even taking into account uncertainties of the refinement of the occupation parameter of a boron position in the presence of a much stronger scatterer such as thulium and difficulties of the quantitative chemical analysis of boron, both experimental results suggest in accord, defects in the boron sublattice. Thereby, no noticeable homogeneity region was found, like it was already observed for $\text{Al}_{0.9}\text{B}_2$ (Ref. 29) or $\text{Mg}_{0.95}\text{B}_2$.³⁰ This behavior is in contrast to such diborides

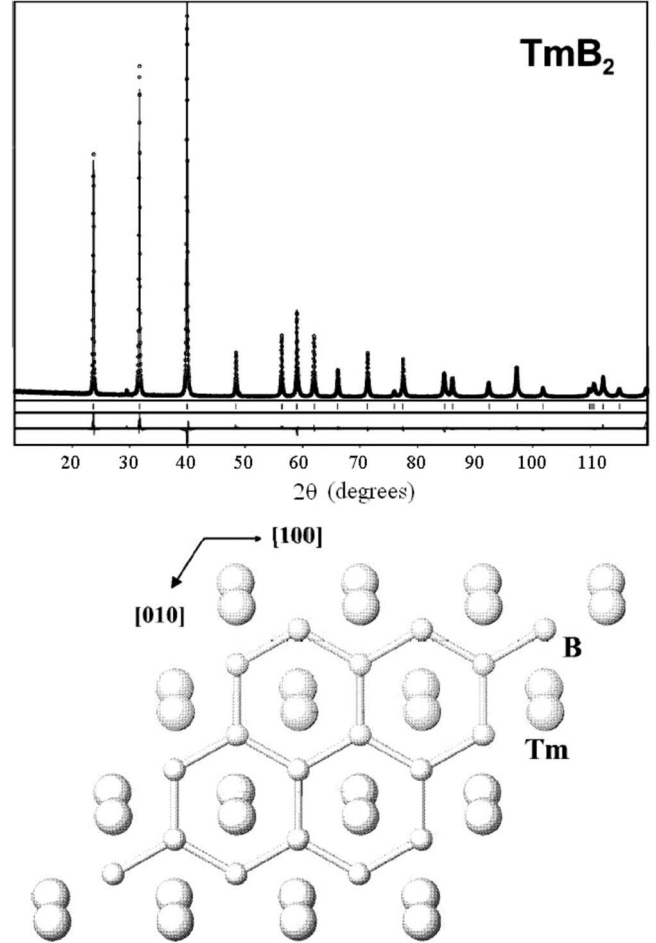


FIG. 1. Crystal structure determination of TmB_2 : (top) X-ray powder-diffraction pattern. Calculated (line) and experimental (points) data are shown together with the difference plot and calculated peak positions (ticks). (bottom) View of the crystal structure along $[001]$. Three-bonded boron atoms form graphitelike layers with $d(\text{B-B})=1.882$ Å.

such as TaB_2 and MoB_2 in which a wide homogeneity region was reported.³¹ The enlarged value for the displacement parameter of Tm is caused by anisotropy ($B_{33} \gg B_{11}$). The anisotropy may correlate with the defects in the boron sublattice. The lattice parameters of LuB_2 were determined as $a=3.2444(3)$ Å and $c=3.7037(5)$ Å.

III. RESULTS AND DISCUSSION

A. Magnetic susceptibility

The temperature dependence of the magnetic susceptibility $\chi(T)$ of TmB_2 is plotted in Fig. 2(a) for magnetic fields of 100 Oe, 1 kOe, and 10 kOe. The behavior with a steep rise of the magnetization below ≈ 8 K and with hysteresis observed below 7 K is typical of a ferromagnetically ordering system. From the peak in the specific heat (presented later), the Curie temperature can be determined as $T_C=7.2$ K.

The inverse magnetic susceptibility $1/\chi(T)=H/M(T)$ is displayed in Fig. 2(b). A Curie-Weiss fit of $\chi(T)$ for $50 \text{ K} \leq T \leq 400 \text{ K}$ yields an effective magnetic moment μ_{eff}

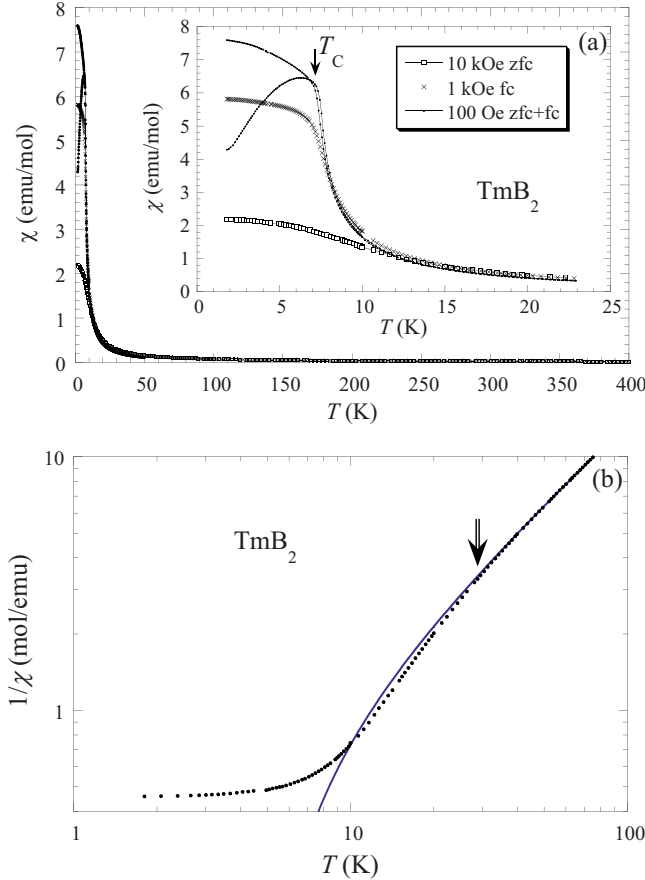


FIG. 2. (Color online) Temperature dependence of the (a) magnetic susceptibility at 100 Oe (dots), 1 kOe (crosses), and 10 kOe (open squares) and (b) inverse magnetic susceptibility at 10 kOe of TmB_2 . In (a) both zero-field-cooled (zfc) and field-cooled (fc) curves are plotted for 100 Oe, while the fc curve is plotted for 1 kOe and the zfc curve for 10 kOe. The line in (b) indicates the $50 \text{ K} \geq T \geq 400 \text{ K}$ fit to the Curie-Weiss law: $1/\chi = (T - \theta_{\text{CW}})/C$, yielding $C = 7.0 \text{ emu K/mol}$ and $\theta_{\text{CW}} = 4.8 \text{ K}$. The arrow indicates the start of the visible deviation at $\approx 30 \text{ K}$.

$= 7.49\mu_B$ and a small positive Weiss temperature $\theta_{\text{CW}} = +4.8 \text{ K}$. The value of μ_{eff} is close to the theoretical value for the $^3\text{H}_6$ multiplet of the free trivalent thulium ion ($7.561\mu_B$).

The magnetic transition temperatures and Weiss temperatures θ_{CW} of diboride compounds are listed in Table I. As mentioned before, the thulium system lies between the ferromagnetic REB_2 ($\text{RE} = \text{Tb, Dy, Ho, Er}$) and the antiferromagnetic YbB_2 , however, now we have made it clear that TmB_2 undergoes a ferromagnetic transition. Antiferromagnetic transitions were observed for the transition-metal diborides MnB_2 (Ref. 32) and CrB_2 .³³ The f -electron dependence of the magnetic behavior of the ferromagnetic REB_2 compounds, including our result for TmB_2 , appears to generally be in line with the Ruderman-Kittel-Kasuya-Yoshida (RKKY) interaction mechanism.³⁴

A clear deviation of $\chi(T)$ from the high-temperature Curie-Weiss behavior is observed below 30 K (Fig. 2(b)). This is due to CEF effects and will be discussed next together with the specific-heat results.

Pulverized and sieved (particle size $< 20 \mu\text{m}$) TmB_2 was aligned in liquid paraffin under a magnetic field of 70 kOe in the SQUID magnetometer and then measured. A reference “random orientation” sample was prepared by fixing the particles in paraffin under zero magnetic field under otherwise identical conditions in the magnetometer. After the measurements x-ray diffraction of the aligned sample showed enhanced intensities of reflections with $(0k0)$ indices and to a lesser extent of $(hk0)$ while displaying almost no intensity for $(00l)$ reflections. This indicates that the easy axis of TmB_2 is in the (001) plane and the spins lie in-plane in the ordered state.

The magnetization curves of both aligned and randomly oriented TmB_2 sample versions for increasing and decreasing fields at 1.8 K are shown in Fig. 3. The aligned sample was measured in a field with the same direction as that of the alignment procedure. A difference is observed between the two samples, indicating the magnetic anisotropy of TmB_2 . The magnetic hysteresis is also observed to be very small. The ordered magnetic moment for the aligned sample reaches a value of approximately $5\mu_B$ at 70 kOe, which is below the full saturation magnetic moment of thulium ($g_J J = 7\mu_B$). This is probably due to the crystal electric field ground state of Tm in TmB_2 (discussed in more detail in Sec. III B on the specific heat) but may be also due to a complex ordering of Tm moments in the (001) plane. The magnetic structure has not been solved in detail yet for any of the

TABLE I. Magnetic parameters of diboride compounds. Effective magnetic moment and Weiss temperature, transition temperature, and kind of magnetic ordering (FM ferromagnetic, AFM antiferromagnetic, WFM weak ferromagnetic).

	μ_{eff}/μ_B	$\theta_{\text{CW}}/\text{K}$	$T_{\text{N/C}}/\text{K}$	Type	Ref.
TbB_2	9.96	+151	151	FM	5
DyB_2	10.7	+33	55	FM	5
HoB_2	10.2	+25	15	FM	5
ErB_2	9.47	+9	16	FM	5
TmB_2	7.49	+4.8	7.2	FM	this work
YbB_2	4.3	-49	5.6	AFM	18
MnB_2	2.3	-	760, 157	AFM, WFM	32
CrB_2	2.1	-700	88	AFM	33

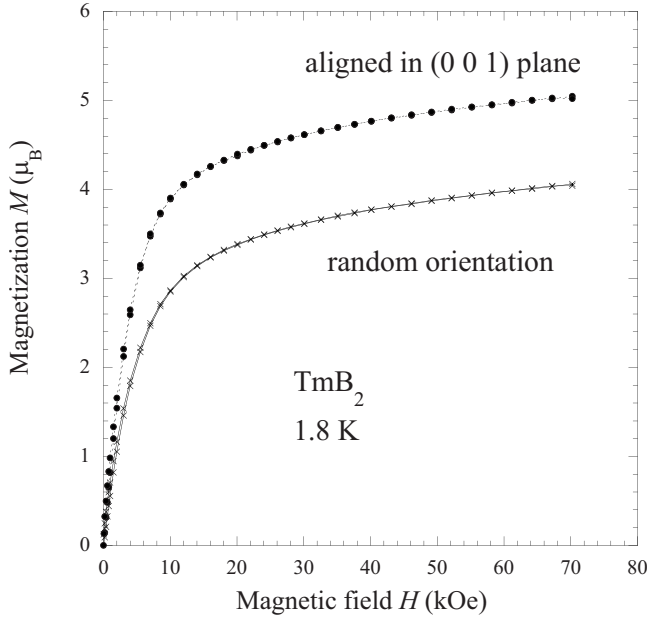


FIG. 3. Magnetization of TmB_2 at 1.8 K for a sample which was aligned in paraffin at 90 kOe (circles) and a randomly oriented fixed sample (crosses).

REB_2 compounds and investigations by neutron experiments should be carried out in the near future on this series of compounds which exhibit ferromagnetism, unusual for rare-earth borides.

B. Specific heat

The specific heat $C_p(T)$ of TmB_2 is shown in Fig. 4. A sharp λ -type peak at $T_C=7.2$ K is observed in $C_p(T)$ indicating that the ferromagnetic transition in TmB_2 is of long-range type. An interesting feature is the hump in $C_p(T)$ in a

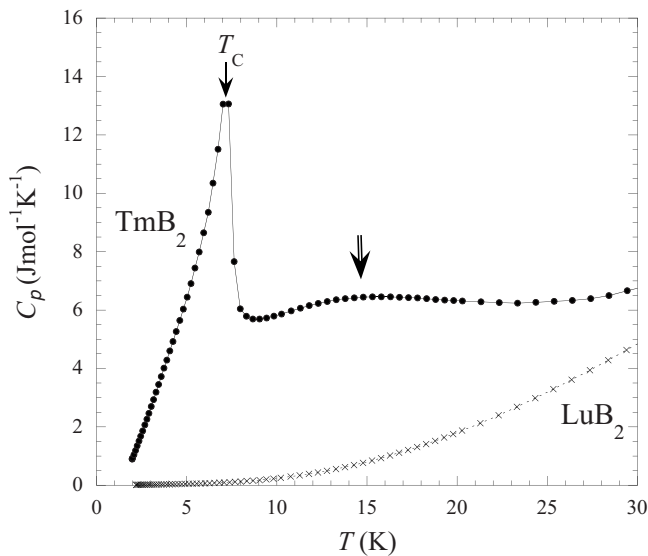


FIG. 4. Temperature dependence of the specific heat C_p of TmB_2 and LuB_2 . The arrows indicate $T_C=7.2$ K and the hump commencing below 30 K.

temperature region significantly higher than T_C , with the hump commencing below ≈ 30 K. As noted above, the inverse susceptibility [Fig. 2(b)] shows a decrease with decreasing temperature, thus deviating from the Curie-Weiss behavior around the same temperature. Both features indicate CEF effects due to the splitting of the $\text{Tm}^{3+} \ ^3\text{H}_6$ multiplet. We exclude that the observed features are due to the presence of a short-range ordering transition at 30 K (as a precursor to the transition at T_C). Complex behavior has only been reported for MnB_2 , which was first found to be a simple ferromagnet at $T_C=157$ K but then later proved by Kasaya *et al.*³² to actually be an antiferromagnet ($T_N=760$ K) with a weak ferromagnetic transition at lower temperatures. However, only relative simple behavior has been reported so far for the known rare-earth diborides REB_2 ($\text{RE}=\text{Tb}, \text{Dy}, \text{Ho}, \text{Er}, \text{Yb}$).

In order to characterize the magnetically ordered state and the CEF we need to determine the magnetic specific heat $C_{\text{mag}}(T)$ and magnetic entropy $S_{\text{mag}}(T)$ of TmB_2 . The specific heat of LuB_2 is a good nonmagnetic lattice reference compound for the magnetic heavy rare-earth diborides; however, it has not been reported yet. Avila *et al.*¹⁸ used an approximation for the lattice heat capacity in their work on YbB_2 . Therefore, LuB_2 was synthesized and the measured specific heat $C_p(T)$ of this compound is also plotted in Fig. 4. The data $T < 9$ K could be described well in the form of a linear electronic specific-heat term and a Debye phonon term: $C_p = \gamma T + \beta T^3$. A fit yields $\gamma = 5.4$ $\text{mJ K}^{-2} \text{mol}^{-1}$ and $\beta = 143$ $\mu\text{J K}^{-4} \text{mol}^{-1}$. The value of γ is not particularly large and the density of states at the Fermi energy for LuB_2 within the free-electron model would be $D(E_F) = 2.3$ states/(eV f.u.). From the coefficient of the phonon term β , the Debye temperature of LuB_2 $\Theta_D(0) = 344$ K is calculated.

For comparison, we consider results previously obtained for LuAlB_4 .²⁰ LuAlB_4 has a structural analogy to LuB_2 , possessing the same metal to boron ratio of $[M]/[B]=1/2$. Whereas LuB_2 has fused hexagonal boron rings sandwiching lutetium atoms, LuAlB_4 has pentagonal and heptagonal rings corresponding to the different-sized lutetium and aluminum atoms embedded between the boron nets. It was determined that $\theta_D = 415$ K for LuAlB_4 . The Debye temperature of LuB_2 is lower than LuAlB_4 , which indicates a lower phonon density of states at lower energies. This could be a reflection of the solely heavy lutetium atomic layer being sandwiched between the planar boron sheets in LuB_2 , compared to LuAlB_4 which has a mixture of light aluminum and lutetium atoms.

Due to the closeness in mass of Tm and Lu, the magnetic specific heat $C_{\text{mag}}(T)$ of TmB_2 was determined by a simple subtraction of the LuB_2 data from the TmB_2 data. The magnetic entropy $S_{\text{mag}}(T)$ is plotted in Fig. 5. An estimate of the entropy below 1.8 K was made by fitting the C_{mag} ($1.97 \text{ K} \leq T \leq 6.2 \text{ K}$) by a power-law function of BT^α ($B = 0.358 \text{ J K}^{-1} \text{mol}^{-1}$, $\alpha = 1.80$) and extrapolation toward zero as shown in the figure.

From the hexagonal symmetry of the Tm site, the $^3\text{H}_6$ Hund's rule multiplet is expected to split into five singlet and four doublet levels (in total 13 states). Figure 5 shows that the magnetic entropy at T_C is about $7.0 \text{ J K}^{-1} \text{mol}^{-1}$, which

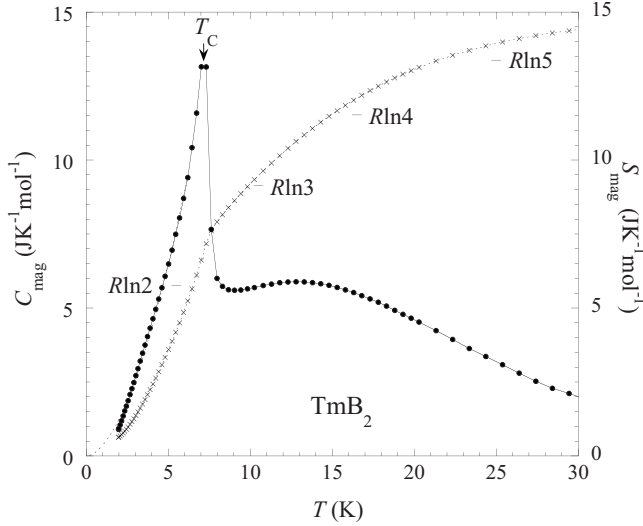


FIG. 5. Temperature dependence of the magnetic specific heat C_{mag} and entropy S_{mag} of TmB_2 . The line depicts the extrapolation of C_{mag} below 1.9 K, which was determined by fitting the $1.97 \text{ K} \leq T \leq 6.2 \text{ K}$ data by a power-law function to obtain parameters of BT^α ($B=0.358 \text{ J K}^{-1} \text{ mol}^{-1}$, $\alpha=1.80$).

is significantly larger than $R \ln 2$ but only 77% of $R \ln 3$. Since usually about 25% of the magnetic entropy is released only by short-range correlations above the long-range ordering temperature (T_C), this indicates that the magnetic order in TmB_2 comprises three states in total. From the magnetic field dependence of $S_{\text{mag}}(T)$ (see below) details on the energy splitting of these three states will be obtained.

$S_{\text{mag}}(T)$ reaches a value of $14.4 \text{ J K}^{-1} \text{ mol}^{-1}$ at 30 K which is about $R \ln 6$. From a comparison with a trial multilevel Schottky anomaly³⁵ for the 13 CEF states one can conclude that these six CEF states need to have energy separations $< k_B \cdot 100 \text{ K}$ from the ground level. This observation confirms that the origin of both the deviation from the Curie-Weiss law in $\chi(T)$ and the hump in $C_p(T)$ are crystal-field effects.

The magnetic field dependence of $C_p(T)$ of TmB_2 is plotted in Fig. 6. The discontinuity due to the long-range magnetic order is already suppressed by application of a field of 10 kOe and the resulting $C_p(T, H)$ curve can be well described by a multilevel Schottky anomaly. As the field increases the energy levels split further due to the Zeeman effect and the maximum of the multilevel Schottky anomaly moves to higher temperatures. From the large amplitude ($\approx 8 \text{ J K}^{-1} \text{ mol}^{-1}$ at 9 K) of the Schottky anomaly for $H = 10 \text{ kOe}$ it can immediately be concluded that the CEF ground level is a singlet (it cannot be a doublet since then maximum would be much lower).³⁵ The two excited states involved in the magnetic order are separated from the ground singlet by about the same energy $\Delta_{12} = k_B \cdot 18 \text{ K}$, thus constituting a doublet or quasidoublet. A small field of order 10 kOe is sufficient to destroy the long-range order by further strong increase in the splitting of these two levels from the ground singlet. A second excited (quasi-)doublet state is situated at a splitting of $\Delta_{13} \approx k_B \cdot 40 \text{ K}$. Due to the complexity of the CEF level scheme and the limited accuracy of $c_{\text{mag}}(T)$ above 30 K we can only unequivocally obtain these lowest-

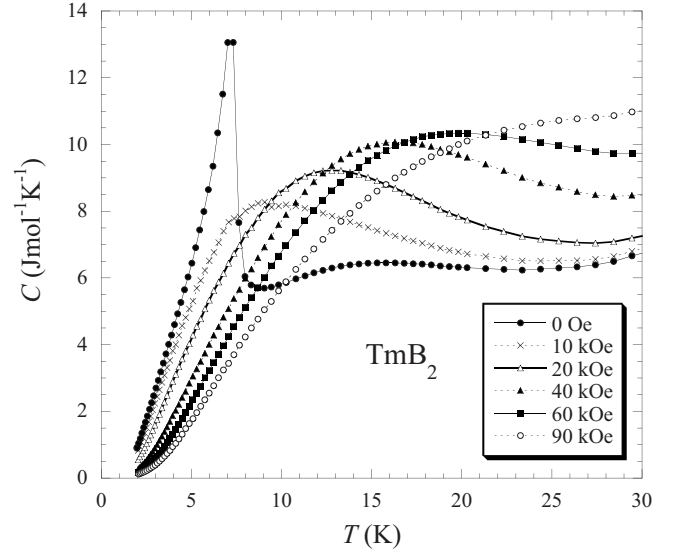


FIG. 6. Temperature dependence of the specific heat $C_p(T, H)$ in various magnetic fields for TmB_2 . 0 Oe (closed circles), 10 kOe (crosses), 20 kOe (open triangles), 40 kOe (closed triangles), 60 kOe (closed squares), and 90 kOe (open circles).

excited CEF levels from the fit with a multilevel Schottky anomaly model.

C. Electronic structure calculations

The starting calculation was performed for the unit cell of nonmagnetic structure with $a = a_{\text{TmB}_2}$ and $c = c_{\text{TmB}_2}$ and complete occupation of the atomic sites [space group $P6/mmm$, Tm in $1a$ (0,0,0), B in $2d$ ($\frac{1}{3}, \frac{2}{3}, \frac{1}{2}$)]. After achieving the self-consistency, the calculations were continued for the larger unit cell with $a = a_{\text{TmB}_2}$ and $c = 2c_{\text{TmB}_2}$ [space group $P6/mmm$, Tm1 in $1a$ (0,0,0), Tm2 in $1c$ (0,0, $\frac{1}{2}$), B in $4h$ ($\frac{1}{3}, \frac{2}{3}, \frac{1}{4}$)]. In this cell the FM and A-type AFM ordering of the Tm atoms along [001] combined with the ferromagnetic interaction within the (001) planes were modeled. Since the Tm atoms form a hexagonal lattice, C-type and G-type antiferromagnetic order will be energetically disfavored due to the strong in-plane frustration in these configurations.³⁶ The total energy of the FM model was found to be lower than that for the AFM model by $\Delta E = 0.029 \text{ mHartree}$, which is equivalent to a temperature of 4.5 K. This energy scale for the magnetic interactions is in good agreement with the measured Curie-Weiss temperature $\theta = +4.8 \text{ K}$ and the FM ordering of the thulium magnetic moments at 7.2 K.

The calculated electronic density of states (Fig. 7, top) shows the localized $4f$ states of Tm well below the Fermi level in the region between -2 eV and -4 eV . They do not mix noticeably with the valence-band states outside this energy window. Thus the $4f$ states are indeed strongly localized and can only interact via an RKKY type of interaction. Direct dipolar coupling of the localized $4f$ moments is expected to be very small and should play only a minor role for the magnetic ordering.

The low-energy bands with $E < -7 \text{ eV}$ are formed mainly by s states of boron and thulium. With increasing energy

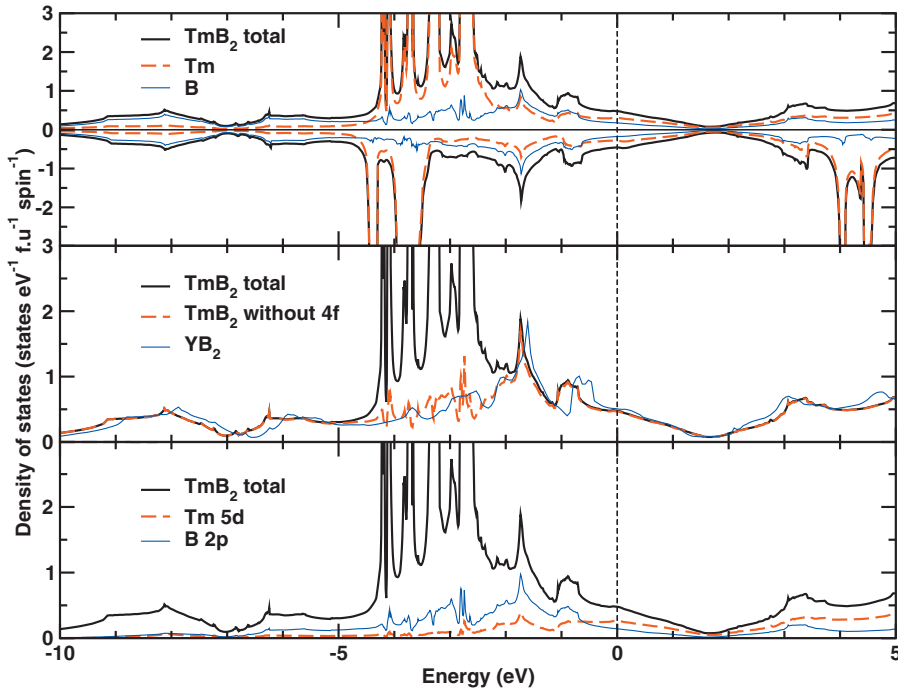


FIG. 7. (Color) Electronic density of states (DOS) for TmB_2 . Total DOS is shown together with the contributions of thulium and boron for spin-polarized states (top). DOS of TmB_2 excluding f states compared with total DOS of YB_2 (middle). Total DOS of TmB_2 plotted with $\text{B}(2p)$ and $\text{Tm}(5d)$ contributions (bottom).

($-7 \text{ eV} < E < E_F$), the contribution of the $\text{B } 2s$ states reduces, the contribution of the $\text{B } 2p$ and $\text{Tm } 5d$ states increases. Two characteristic DOS peaks at $E = -1 \text{ eV}$ and $E = -2 \text{ eV}$ are typical features of the RE diborides: the DOS for YB_2 (Fig. 7, middle) shows a very similar structure between -1 and -2 eV as the DOS for TmB_2 excluding the remaining small $4f$ -state contributions (Fig. 7, middle). So the DOS at E_F is composed mostly of $\text{B}(2p)$ and $\text{Tm}(5d)$ states (Fig. 7, bottom). The sizeable contribution of the $\text{Tm}(5d)$ states to the DOS at the Fermi level is in line with the suggested RKKY-type magnetic interaction since these states also show a significant spin polarization (Fig. 7, top). As expected, a spin-polarized calculation for the parent compound YB_2 yields a nonmagnetic ground state.

IV. CONCLUSIONS

TmB_2 was successfully synthesized and the magnetic properties investigated. It adapts the crystal structure of the AlB_2 type with small deficiency of the boron sublattice. A ferromagnetic transition was observed at $T_C = 7.2 \text{ K}$ reveal-

ing that the thulium phase is in line with the ferromagnetic order observed for REB_2 ($RE = \text{Tb, Dy, Ho, Er}$) rather than the antiferromagnetic transition in YbB_2 . Measurements on an aligned sample indicate that the easy-axis direction is within the (001) plane and the spins lie in-plane in the ordered state. With the determined magnetic specific heat and entropy the crystal field of the 3H_6 multiplet of Tm in TmB_2 was investigated and a singlet ground state was found while the magnetic ordering involves three CEF levels.

Band-structure calculations on TmB_2 were performed with FPLO within LSDA comparing FM order and antiferromagnetic (AFM) ordering along $[001]$ combined with ferromagnetic interaction within the (001) plane. The FM ordered state is more stable than AFM ordering. REB_2 are unusual among the rare-earth borides in that they exhibit ferromagnetism and study of the detailed magnetic structures of REB_2 compounds by neutron experiments should be carried out in the future.

ACKNOWLEDGMENT

L. Craco is thanked for helpful discussions.

*mori.takao@nims.go.jp

¹T. Mori, in *Handbook on the Physics and Chemistry of Rare Earths*, edited by K. A. Gschneidner, Jr., J.-C. Bunzli, and V. Pecharsky (North-Holland, Amsterdam, 2008) Vol. 38, p. 105.

²B. T. Matthias, T. H. Geballe, K. Andres, E. Corenzwit, G. W. Hull, and J. P. Maita, *Science* **159**, 530 (1968).

³J. Etourneau, *J. Less Common Met.* **110**, 267 (1985).

⁴D. Gignoux and D. Schmitt, in *Handbook of Magnetic Materials*, edited by K. H. J. Buschow (North-Holland, Amsterdam, 1997)

Vol. 10, p. 239.

⁵K. H. J. Buschow, *Boron and Refractory Borides* (Berlin, Heidelberg, 1977) p. 494.

⁶K. Siemensmeyer, E. Wulf, H.-J. Mikeska, K. Flachbart, S. Gabani, S. Mat'as, P. Priputen, A. Efdokimova, and N. Shitsevalova, *Phys. Rev. Lett.* **101**, 177201 (2008).

⁷R. Watanuki, H. Mitamura, T. Sakakibara, G. Sato, and K. Suzuki, *Physica B* **378-380**, 594 (2006).

⁸S. Michimura, A. Shigekawa, F. Iga, M. Sera, T. Takabatake, K.

- Ohoyama, and Y. Okabe, *Physica B* **378-380**, 596 (2006).
- ⁹T. Mori and T. Tanaka, *J. Phys. Soc. Jpn.* **68**, 2033 (1999).
- ¹⁰T. Mori, *J. Appl. Phys.* **95**, 7204 (2004).
- ¹¹T. Mori, *J. Appl. Phys.* **99**, 08J309 (2006).
- ¹²T. Mori and A. Leithe-Jasper, *J. Appl. Phys.* **93**, 7664 (2003).
- ¹³T. Mori and H. Mamiya, *Phys. Rev. B* **68**, 214422 (2003).
- ¹⁴T. Mori and A. Leithe-Jasper, *Phys. Rev. B* **66**, 214419 (2002).
- ¹⁵T. Mori, F. Zhang, and A. Leithe-Jasper, *J. Solid State Chem.* **177**, 444 (2004).
- ¹⁶T. Mori and F. Zhang, *J. Phys.: Condens. Matter* **14**, 11831 (2002).
- ¹⁷T. Mori and T. Tanaka, *J. Alloys Compd.* **288**, 32 (1999).
- ¹⁸M. A. Avila, S. L. Bud'ko, C. Petrovic, R. A. Ribeiro, P. C. Canfield, A. V. Tsvyashchenko, and L. N. Fomicheva, *J. Alloys Compd.* **358**, 56 (2003).
- ¹⁹T. Mori, S. Okada, and K. Kudou, *J. Appl. Phys.* **97**, 10A910 (2005).
- ²⁰T. Mori, H. Borrmann, S. Okada, K. Kudou, A. Leithe-Jasper, U. Burkhardt, and Yu. Grin, *Phys. Rev. B* **76**, 064404 (2007).
- ²¹K. Koepf and H. Eschrig, *Phys. Rev. B* **59**, 1743 (1999).
- ²²J. P. Perdew and Y. Wang, *Phys. Rev. B* **45**, 13244 (1992).
- ²³M. T. Czyżyk and G. A. Sawatzky, *Phys. Rev. B* **49**, 14211 (1994).
- ²⁴W. Schnelle, A. Leithe-Jasper, M. Schmidt, H. Rosner, H. Borrmann, U. Burkhardt, J. A. Mydosh, and Y. Grin, *Phys. Rev. B* **72**, 020402(R) (2005).
- ²⁵H. Eschrig, *Optimized LCAO Method and the Electronic Structure of Extended Systems* (Springer, Berlin, 1989).
- ²⁶P. Rogl and H. Klesnar, *J. Solid State Chem.* **98**, 99 (1992).
- ²⁷R. N. Castellano, *Mater. Res. Bull.* **7**, 261 (1972).
- ²⁸J. F. Cannon, D. M. Cannon, and H. T. Hall, *J. Less-Common Met.* **56**, 83 (1977).
- ²⁹U. Burkhardt, V. Gurin, F. Haarmann, H. Borrmann, W. Schnelle, A. Yaresko, and Yu. Grin, *J. Solid State Chem.* **177**, 389 (2004).
- ³⁰J. Schmidt, W. Schnelle, Yu. Grin, and R. Kniep, *Solid State Sci.* **5**, 535 (2003).
- ³¹A. S. Sobolev, Yu. B. Kuzma, T. E. Soboleva, and T. F. Federov, *Powder Metall. Met. Ceramics* **7**, 48 (1968).
- ³²M. Kasaya and T. Hihara, *J. Phys. Soc. Jpn.* **29**, 336 (1960).
- ³³S. H. Liu, L. Kopp, W. B. England, and H. W. Myron, *Phys. Rev. B* **11**, 3463 (1975).
- ³⁴M. A. Ruderman and C. Kittel, *Phys. Rev.* **96**, 99 (1954); T. Kasuya, *Prog. Theor. Phys.* **16**, 45 (1956); K. Yosida, *Phys. Rev.* **106**, 893 (1957).
- ³⁵A. Tari, *The Specific Heat of Matter at Low Temperatures* (Imperial College Press, London, 2003); E. S. R. Gopal, *Specific Heat at Low Temperatures* (Plenum, London, 1966).
- ³⁶For computational reasons, only commensurate magnetic structures have been considered. An extension of the computational investigations to the incommensurate wave vectors is left for future studies.